A novel citrate synthase isoform contributes infection and stress resistance of the stripe rust fungus

Dan Li[1†], Lijing Pang[1†], Pu Yuan[1], Peijing Zheng[1], Baoyu Huai[2], Mohan Yao[2], Zhensheng Kang[2*], Jie Liu[1*]

[1] State Key Laboratory of Crop Stress Biology for Arid Areas and College of Life Sciences, Northwest A&F University, Yangling, PR China

[2] State Key Laboratory of Crop Stress Biology for Arid Areas and College of Plant Protection, Northwest A&F University, Yangling, PR China

* For correspondence. E-mail: liujie2003@hotmail.com; Tel. (+86) 02987092262; Fax (+86) 02987092262.

E-mail: kangzs@nwsuaf.edu.cn; Tel. (+86) 02987080061; Fax (+86) 02987080061

[†]These authors contributed equally to this work.

A running title: Characterization of a citrate synthase PsCS1

This article has been accepted for publication and undergone full peer review but has not been through the copyediting, typesetting, pagination and proofreading process, which may lead to differences between this version and the Version of Record. Please cite this article as doi: 10.1111/1462-2920.14444

Summary

The early development of a rust fungus is dependent on the endogenous lipids stored in the urediniospores. After it establishes a parasitic relationship with the host, sugars absorbed from the host cells by haustoria become the primary nutrients. The tricarboxylic acid (TCA) cycle is essential to oxidize these nutrients. However, few studies have addressed the role of citrate synthase (CS), a rate-limiting enzyme of the TCA cycle, during the infection process of rust fungi. In this study, a CS gene from *Puccinia striiformis* f. sp. *tritici* (*Pst*), *PsCS1*, was cloned and characterized. Transcripts of *PsCS1* and the enzyme activity of the CS were increased in the early *Pst* infection stage. Biochemical features and subcellular localization revealed that *PsCS1* encoded a mitochondrial CS. Size exclusion chromatography, yeast two-hybrid and bimolecular fluorescence complementation experiments confirmed that PsCS1 could form a functional homo-octamer. The overexpression of *PsCS1* enhanced the resistance of *Escherichia coli* to salt stress. The knockdown of *PsCS1* using a host-induced gene silencing (HIGS) system blocked *Pst* growth in wheat. These results indicate that PsCS1 is required for nutrient metabolism in *Pst* and contributes to *Pst* infection by regulating ATP production and the supply of carbon sources.

Introduction

The tricarboxylic acid (TCA) cycle is an essential metabolic network in all oxidative organisms and provides the carbon skeletons for many biosynthetic processes and reducing factors, such as NADH and FADH2, which drive the generation of ATP (Chen *et al*., 2011). The TCA cycle occurs in the mitochondrial matrix of eukaryotic cells and the cytoplasm of prokaryotic cells. Citrate synthase (CS), which catalyzes the condensation of acetyl-coenzyme (acetyl-CoA) and oxaloacetate (OAA) to form citrate, is the rate-limiting enzyme of the TCA cycle (Schmidtmann *et al*., 2014).

Citrate synthases are composed of several isoforms with distinct biochemical characteristics and subcellular localization. Isoforms of eukaryotic CSs can be found in the mitochondria (mCSs), glyoxysomes (gCSs), and peroxisomes (pCSs) (Schnarrenberger and Martin, 2002). Phylogenetic analysis reveals that mCSs from animals, plants, and fungi along with fungal pCSs are closely related and are evolutionarily distinguished from the CSs of other organisms. Therefore, it is reasonable to assume that the pCSs evolved due to duplication of the mCS-encoding gene during the evolution of fungi. In contrast, the gCS-encoding gene may have been acquired from eubacteria. Eukaryotic CSs seem to be more similar to eubacterial than to archaebacterial homologs (Schnarrenberger and Martin, 2002).

Currently, many CS genes have been cloned from bacteria, fungi and other higher eukaryotes, such as *Escherichia coli* (Guest, 1981), *Saccharomyces cerevisiae* (Kim *et al*., 1986; Rosenkrantz *et al*., 1986; Suissa *et al*., 1984), *Neurospora crassa* (Ferea *et al*., 1994), *Aspergillus nidulans* (Park *et al*., 1997), *Arabidopsis thaliana* (Unger *et al*., 1989) and humans (Goldenthal *et al*., 1998). Increasing evidence suggests that the CS activity exerts an influence on

various kinds of metabolic processes. For example, in *E. coli*, the CS (gltA)-deficient mutant fails to grow on minimal medium with glucose as the sole carbon source unless L-glutamate or L-proline (which is catabolized to L-glutamate) was supplemented (Guest, 1981). Two CS isoforms of *Staphylococcus aureus*, CitZ and SbnG, contribute citrate to the formation of staphyloferrin A and staphyloferrin B to enhance growth under iron-restriction, respectively (Sheldon *et al*., 2014). In *S. cerevisiae*, three CS isoforms (Cit1p, Cit2p and Cit3p) are encoded by different nuclear genes. Cit1p, the primary mitochondrial CS, serves as the rate-limiting enzyme of the TCA cycle (Suissa *et al*., 1984). Cit2p is involved in the glyoxylate cycle and/or biosynthesis of glutamate in peroxisome (Kim *et al*., 1986; Lewin *et al*., 1990; Rosenkrantz *et al*., 1986). *Cit3p* is poorly expressed under normal conditions and it is required for growth on glycerol in the presence of a CIT1 deletion (Jia *et al*., 1997). In *A. nidulans*, the expression of the *citA* gene encoding the mitochondrial CS is up-regulated in cleistothecial shells, but significantly weak in the contents of the cleistothecia including ascospores. Acetate strongly induced *citA* expression, which is subjected to carbon catabolite repression caused by glucose (Min *et al*., 2010).

Citrate synthases are also involved in a variety of physiological processes in plants, such as mitochondrial energy metabolism, seed germination, and stress tolerance. For example, Pracharoenwattana *et al*. (2005) found that the peroxisomal CS is required for fatty acid respiration and seed germination in *Arabidopsis*. Additionally, some studies have indicated that plants can increase the availability of soil phosphorus by secreting citric acid to activate insoluble inorganic phosphorus in the soil. In *Arabidopsis*, the overexpression of the mitochondrial CS from *Daucus carota* improved growth on a phosphorus-limited soil (Koyama *et al*., 2000). Transgenic

pigeonpea plants overexpressing a *D. carota* CS gene can acquire more phosphorus under phosphorus deficient conditions (Aftab Hussain *et al*., 2016). Similarly, CS can also enhance tolerance to aluminum toxicity in acidic soils as one of the major limiting factors for the growth of crops. For example, tobacco and papaya plants overexpressing a *Pseudomonas aeruginosa* CS have been reported to exhibit enhanced tolerance to aluminum (de la Fuente *et al*., 1997). Barone *et al.* (2008) introduced the CS gene from *P. aeruginosa* to alfalfa. The results showed that the tolerance of transgenic alfalfa to acid soil and aluminum toxicity was significantly enhanced, and the yield of the plants was significantly increased. The overexpression of a mitochondrial CS gene from *A. thaliana* improves the growth of carrot cells in Al-phosphate medium (Koyama *et al*., 1999). In addition, Tong *et al.* (2009) found that the CS gene from *Brassica napus* responded to water logging, drought, and sclerotium blight, as well as different hormone treatments. The expression of the CS gene from *Sinapis alba* was up-regulated when the plants were under drought stress (Yue *et al*., 2014).

Stripe rust is one of the most destructive wheat diseases and continues to threaten worldwide wheat production and global food security. This disease is caused by *Puccinia striiformis* f. sp. *tritici* (*Pst*), which is an obligate biotrophic fungus undergoing a complex life cycle and differentiating a highly sophisticated series of infection structures (Zhao *et al*., 2016). *Pst* must obtain nutrients from its host for cell metabolism and biosynthesis. The TCA cycle is a central metabolic hub necessary for ATP production and to provide the precursors used in many biosynthetic pathways. However, the role of CS, a pace-making enzyme of the TCA cycle, remains unclear in *Pst* nutrient metabolism. Based on previous transcriptome sequencing of *Pst*-infected wheat seedlings, we cloned a *Pst* CS gene, designated *PsCS1*, and characterized its

expression at different infection stages of *Pst*. Subcellular localization and biochemical features were determined using heterologous systems. In addition, overexpression and knockdown of *PsCS1* were performed to identify its functions during *Pst* infection. Our results indicate that *PsCS1* contributed to the *Pst* infection of wheat by regulating the supply of carbon sources and energy in *Pst.*

Results

Cloning, sequencing, and characterization of *PsCS1*

A cDNA sequence orthologous to CS, designated *PsCS1*, was isolated from a *Pst*-infected wheat transcriptome (Hao *et al*., 2016). The PsCS1 gene, a single copy in the *Pst* genome, was PCR-amplified, and sequencing analysis showed that it consisted of 2,167 bases and contained eight introns. The intron-length polymorphisms (84, 77, 78, 75, 82, 100, 102 and 93 bases) were displayed. The full-length open reading frame (ORF) nucleotide sequence of *PsCS1*, which consists of 1,476 nucleotides, encodes a 491-amino acid polypeptide with a calculated molecular weight of 55,001 Da, a theoretical isoelectric point (pI) of 9.14, and a CS domain.

We used the PsCS1 sequence as a query to perform similarity search against the non-redundant protein sequence databases. The results showed that the highest sequence similarities were found to homologous proteins from other fungi. Likewise, similarities to homologous proteins from plants were also shown (data not shown). The PsCS1 protein sequence shows 90% identity with the CS from *P. triticina* 1-1 BBBD Race 1 (GenBank Accession No. OAV98913), 89% identity with the CS from *P. graminis* f. sp. *tritici* CRL 75-36-700-3 (GenBank Accession No. XP_003328509), 84% identity with the CS from *P. sorghi* (GenBank Accession No. KNZ53414) and 83% identity with the CS from *Melampsora larici-populina* 98AG31

(GenBank Accession No. XP_007416968). The phylogenetic relationships of PsCS1 with the CSs from other basidiomycetous and ascomycetous fungi are exhibited in Supporting Information Fig. S1. PsCS1 had a greater sequence similarity to the CSs from basidiomycetous fungi, especially rust fungi, than to ascomycetous fungi. PsCS1 displayed the highest amino acid sequence homology with the CS protein of *P. triticina*.

***PsCS1* expression pattern and citrate synthase activity**

The *PsCS1* transcript levels were assayed at various stages of *Pst* infection using qRT-PCR. The results showed that *PsCS1* was expressed differentially in nongerminated urediniospores and *Pst*-infected wheat leaves sampled from 6 to 264 hours post inoculation (hpi). In nongerminated urediniospores, the *PsCS1* expression level was relatively low. However, the *PsCS1* transcript abundance was increased at 6 hpi and then remained at a high level until 48 hpi (Fig. 1A). During the later *Pst* infection stages, the expression of *PsCS1* was down-regulated (Fig. 1A).

In addition, the CS enzyme activity in nongerminated and germinated urediniospores was determined. The results showed that the enzyme activity significantly increased upon germination compared with nongerminated urediniospores (Fig. 1B), which was consistent with the transcription pattern of *PsCS1*.

Enzymatic characterization of PsCS1

The soluble Trx-PsCS1 fusion protein was expressed in the cultures of *E. coli* BL21(DE3) harboring the recombinant plasmid pET32a-*PsCS1*, and purified to a single protein band by Ni-NTA affinity and ion-exchange chromatography, as shown in the Coomassie blue-stained SDS-PAGE gel (Fig. 2A). The electrophoretic migration of the recombinant PsCS1 was consistent with the estimated molecular weight of approximately 70 kDa (Fig. 2A). The protein was further

identified by Western blotting using anti-His monoclonal antibody, and the Trx tag alone (~20 kDa) and the Trx-PsCS1 fusion protein (~70 kDa) were exhibited in Supporting Information Fig. S2.

A biochemical characterization of PsCS1 was conducted. The optimum temperature was determined to be approximately 20°C. An elevation in temperatures led to a rapid loss of enzyme activity (Fig. 2B). The optimal pH value was approximately pH 8.0 (Fig. 2C). Additionally, metal cations also exerted differential effects on the enzyme activity of PsCS1. The inclusion of 0.5 mM K^+ in the reaction mixture increased the enzyme activity by 25% (Fig. 2D). The enzyme activity of PsCS1 was partially inhibited by Fe^{3+}, Zn^{2+}, Cu^{2+} and Mn^{2+} (Fig. 2D). The addition of Cu^{2+} decreased the enzyme activity of PsCS1 by 87% (Fig. 2D).

PsCS1 forms homo-octamers independent of disulfide bonds

To investigate the polymerization of PsCS1, size exclusion chromatography was used, and the native molecular weight of PsCS1 was determined to be 494.77 kDa (Supporting Information Fig. S3, Fig. 3A), which was approximately eight times as high as that of the PsCS1 monomer. To further identify the self-interaction of PsCS1 using a yeast two-hybrid system, PsCS1 fused with GAL4 DNA-binding domain was used as the bait, and PsCS1 coupled with GAL4 activation domain served as the prey. After cotransformation of the bait and prey plasmids into yeast cells, the interactions were assessed by the survival of yeast on histidine-deficient media and the production of β-galactosidase. As shown in Fig. 3B, reporter activation suggested that PsCS1 interacted with itself. In addition, the interactions between PsCS1 proteins were assayed by bimolecular fluorescence complementation (BiFC), a technique that allows the interaction of proteins to be observed in vivo, in transiently transformed tobacco leaves. The results revealed that strong green fluorescent protein (GFP) signals were detected when agrobacteria containing

pSPYNE(R)173-*PsCS1* or pSPYCE(M)-*PsCS1* were co-infiltrated into tobacco leaves (Fig. 3C). However, no fluorescence was visualized when agrobacteria carrying pSPYNE(R)173-*PsCS1* or the empty pSPYCE(M) vector were co-infiltrated (Fig. 3C), indicating that PsCS1 could form homo-octamers by self-interaction.

In addition, the amino acid constitution of PsCS1 was analyzed using the ProtParam tool. The results showed that PsCS1 contains none of the cysteine required for disulfide bond formation (Supporting Information Fig. S4). Thus, it is inferred that the polymerization of PsCS1 is independent of disulfide bonds.

Subcellular localization of PsCS1

To determine the subcellular localization of PsCS1, transient expression analysis of the PsCS1-GFP fusion protein in *Nicotiana benthamiana* leaves was performed. The distribution pattern of numerous small spots suggested that PsCS1 was possibly localized in the mitochondria or peroxisome. To test this hypothesis, the PsCS1-GFP fusion protein was transiently expressed in *N. benthamiana* leaves together with a mitochondrial (cd3-991) or peroxisomal organelle marker (cd3-983). The results showed that PsCS1-GFP strongly co-localized with the mCherry-labelled mitochondrial marker (Fig. 4), while no co-localization was observed when the PsCS1-GFP fusions were expressed along with a peroxisomal marker (Fig. 4). Thus, these observations suggest that PsCS1 is a mitochondria-localized protein.

Overexpression of *PsCS1* in *E. coli* enhances its growth under salt stress

The *E. coli* cells carrying the recombinant plasmid pET32a-*PsCS1* or the empty pET32a vector were spotted on the LB basal media containing 50, 150, and 250 mM NaCl, respectively. Different growth was observed on the LB plates after overnight incubation. The *PsCS1*-expressed

cells were able to tolerate high salt concentrations (Fig. 5A). In contrast, the growth of the cells harboring the empty vector was significantly inhibited (Fig. 5A). In addition, the cell growth under salt stress was also determined in LB liquid media. The cells transformed with recombinant pET32a-*PsCS1* plasmid displayed rapid growth in LB media containing 250 mM NaCl, while the cells with the vector alone grew slowly (Fig. 5B).

A similar assay was conducted to determine the response of *E. coli* containing the recombinant plasmid pET32a-*PsCS1* or the empty vector pET32a to PEG, H_2O_2 and temperature stress. The results showed that no obvious difference in growth rate was observed between the *E. coli* cells expressing the PsCS1 protein and the control when H_2O_2 (Supporting Information Fig. S5A) or PEG (Supporting Information Fig. S5B) was added to the media, respectively. In addition, low-temperature tolerance of *E. coli* cells with PsCS1 was not significantly enhanced compared with the control (Supporting Information Fig. S5C). It seemed that the protein PsCS1 expressed in *E. coli* cells did not increase the growth ability in these abiotic stresses.

Silencing of *PsCS1* by HIGS reduces fungal biomass at the middle stage of *Pst* infection

There is presently no effective transformation system to identify gene functions for rust fungi. Therefore, the host-induced gene silencing (HIGS) technique mediated by barley stripe mosaic virus (BSMV) was exploited to knockdown the *PsCS1* expression in *Pst*. Chlorotic and mosaic symptoms were observed in BSMV-inoculated wheat seedlings at 9 days post inoculation (dpi), and these plants showed no obvious growth defects (Fig. 6A). In the *TaPDS* (wheat phytoene desaturase gene)-silenced wheat leaves, an expected photo-bleaching phenotype was visualized at 15 dpi (Fig. 6A), demonstrating that the BSMV-mediated HIGS system worked correctly in wheat. The fourth leaves of BSMV-inoculated wheat plants were infected with CYR31. The results

showed that *Pst* with the decreased *PsCS1* transcription remained virulent enough to cause a full susceptible phenotype of wheat and the rust disease phenotypes exhibited no significant change compared with the control plants at 15 dpi (Fig. 6B).

To test whether the sporulation phenotypes observed were correlated with mycelial growth in the host tissues, fungal biomass was measured using the BSMV:*PsCS1*-inoculated leaves superinfected with *Pst*. Total DNA was extracted and the relative levels of *PsEF1* (the *Pst* gene) and *TaEF-1a* (the wheat gene) were calculated using real-time quantitative PCR on basis of the standard curves constructed (Liu *et al*., 2016). At 15 dpi, there was no significant difference in the fungal biomass between the *PsCS1*-silenced wheat plants and the BSMV:γ-inoculated controls (Supporting Information Fig. S6), which was consistent with the disease phenotypes observed. However, at 7 dpi the fungal biomass in the wheat leaves infected by BSMV:*PsCS1*-as1 and BSMV:*PsCS1*-as2 was decreased by 33% and 42%, respectively (Fig. 6C). This result suggested that fungal growth was restricted at this stage, probably as a result of the nutrient supply attenuation triggered by the silencing of *PsCS1*.

To determine whether *PsCS1* was effectively silenced, the relative transcript level of *PsCS1* was assayed using qRT-PCR in the fourth leaves inoculated with *Pst*. The results showed that the *PsCS1* transcript in the BSMV:*PsCS1*-as1-inoculated wheat leaves was reduced by 64%, 53%, and 49% at 24, 48, and 120 hpi, respectively; in the BSMV:*PsCS1*-as2-inoculated leaves, the transcript abundance of *PsCS1* was decreased by 57%, 62%, and 58%, respectively, compared with the wheat leaves infected by BSMV:γ (Fig. 6D). These results suggest that the *PsCS1* expression was significantly knockdowned by BSMV-HIGS. In addition, the expression of two wheat CS genes *TaCS1* and *TaCS2* was also measured by qRT-PCR in the HIGS plants. The results showed that no

significant difference was observed compared with the control (Supporting Information Fig. S7A and B), indicating that silencing of *PsCS1* by HIGS had no influence on the CS gene expression in the wheat plants.

HIGS of *PsCS1* restricts *Pst* growth and development

To clarify the role of *PsCS1* in pathogenicity of *Pst*, the fungal development in the HIGS wheat plants infected with *Pst* was assessed. At 24 and 48 hpi, the number of haustorial mother cells, haustoria and hyphal branches in the BSMV:*PsCS1*-inoculated wheat seedlings showed little difference compared with the control (Fig. 7A, B, D, E and G; Supporting Information Fig. S8A). In addition, the hyphal length were also similar to those of the controls (P>0.05) at 24 and 48 hpi (Supporting Information Fig. S8B and C). However, compared with the control, the colonization and formation of the secondary hyphae were significantly impeded in the HIGS wheat plants at 120 hpi (Fig. 7C, F and H).

Discussion

Although CSs are well known to play pivotal roles in energy production and in providing important biosynthetic precursors, few studies have focused on the characteristics of fungal CSs, except for several citric acid-producing fungi that are used industrially. In this study, a *Pst* CS gene *PsCS1* was cloned, and its expression pattern and biochemical features were characterized. In addition, the function of *PsCS1* was identified through heterologous overexpression and a BSMV-HIGS system. The results indicate that *PsCS1* encodes a mitochondria-localized CS and contributes to *Pst* infection and stress resistance.

Previous studies have found that the CS genes are up-regulated in many fungi during vegetative growth or infection, such as *A. nidulans* (Min *et al*., 2010), *A. oryzae* (Maeda *et al*.,

2004), *S. aureus* (Sheldon *et al*., 2014) and *Paracoccidioides brasiliensis* (Bastos *et al*., 2007). In this study, the *PsCS1* transcript abundance was increased at the early infection stage. Consistent with the high levels of *PsCS1* transcripts, high CS enzyme activity was detectable in the germinated urediniospores compared with the nongerminated urediniospores. Before haustoria form, *Pst* is dependent upon the lipids stored in urediniospores, which are then converted into carbohydrates by the glyoxylate cycle for development (Liu *et al*., 2014). In addition, the TCA cycle also becomes more active to satisfy the energy requirements. Thus, it is reasonable that high CS enzyme activity was assayed during *Pst* germination. Once a parasitic relationship with the host was established, sugars and amino acids were obtained from the host cells by haustoria (Voegele and Mendgen, 2003). The TCA cycle ran at a relatively low rate at this stage.

The major forms of CSs are divided into two types based on their regulatory and structural properties. Type I CSs exist in Gram-positive bacteria, archaea and eukaryotes, and form dimers (60-100 kDa) of identical subunits (approximately 45 kDa). The dimer can be reversibly denatured to inactive monomers. Each subunit contributes functional groups to the active site of the other (Schnarrenberger and Martin, 2002; Weitzman and Jones, 1968). In contrast, type II CSs are only found in Gram-negative bacteria. This kind of CSs forms hexamers (a trimer of dimers) and their molecular masses range between 240 and 280 kDa or greater (Weitzman and Dunmore, 1969). Here, the polymerization of PsCS1 was determined using size exclusion chromatography. Interestingly, the molecular weight is approximately eight times as high as that of the PsCS1 monomer. Therefore, we hypothesize that PsCS1 potentially forms an octamer, which differs from the previously reported CSs from other species, indicating that *PsCS1* probably encodes a novel CS. Subsequent yeast two-hybrid and BiFC experiments confirmed that PsCS1 could interact with

itself, further validating the polymerization of PsCS1 in vivo. These results suggest that PsCS1 functions as a homo-octamer.

Numerous studies have demonstrated that eukaryotic CSs are similar in genetic and biochemical aspects (Alekseev *et al*., 2016). However, the kinetic characteristics of CSs still exhibit some variation, depending on the taxonomic affiliation of the organism, although they can be caused partly by various technological and methodological designs of the experiments. In the present study, PsCS1 was characterized biochemically. We found that PsCS1 belongs to a cold-active enzyme, which is possibly involved in the atypical living environment of *Pst*. The *Pst* infection of host plants requires temperature lower than 23°C (Zhao *et al*., 2016). In addition, pH and metal ions exert a significant influence on the enzymatic activity of PsCS1. Because PsCS1 contains no cysteine, the formation of a PsCS1 homo-octamer is independent of disulfide bonds. Thus, the enzymatic activity of PsCS1 is possibly affected, because the PsCS1 homo-octamer is depolymerized and inactivated by the inappropriate pH as described previously by Mcevily and Harrison (1986). The inhibition by higher concentrations of metal ions is commonly thought to be due to the chelation between the metal ions and the polyphosphate chain of the acetyl-CoA molecule (Kosicki and Lee, 1966).

Environmental stress elicits diverse responses at the physiological, biochemical, cellular and developmental levels (Vargas *et al*., 2007). Acceleration of the TCA cycle is considered as an early response to meet the high-energy requirement and biosynthesis of necessary compounds to cope with unfavorable situations. Therefore, CSs play a key role when organisms are subjected to abiotic and biotic stresses. Recent studies have indicated that the expression of CS is affected by a series of abiotic stress factors such as waterlogging, drought, and salinity (Kang *et al*., 2010; Tong

et al., 2009; Yue *et al*., 2014; Zhao *et al*., 2014). In this study, the overexpression of *PsCS1* in *E. coli* enhanced the resistance of recombinant cells to salt stress. However, no significant difference in the growth rate was observed between the *PsCS1* overexpression strain and the control under PEG, H_2O_2 and cold stresses. Therefore, we speculate that unidentified metabolites of the TCA cycle confer *E. coli* with enhanced resistance to salt stress. Alternatively, increased ATP production due to the overexpression of *PsCS1* may improve the excretion of cytoplasmic sodium ions, because sodium pump activity is dependent on ATP. Another possibility is that the accumulation of intracellular organic acids, intermediate metabolites of the TCA cycle, can increase osmotic potentials, while accompanied water uptake favors the salt tolerance of cells. Thus, it is a reasonable inference that high CS activity could be correlated with the adaptation of *Pst* to unfavorable environmental conditions during infection.

Citrate synthase is a key enzyme responsible for condensation of OAA and acetyl CoA to produce citrate in mitochondria. In addition to direct synthetic function, CS also regulates TCA, the β-oxidation of fatty acids, and participates in the photorespiratory glycolate pathway in plants (Liu *et al*., 2013). Therefore, CS plays a central metabolic role in many aerobic organisms. In this study, a BSMV-HIGS approach was used to determine the role of *PsCS1* during *Pst* infection. The restricted hyphal spread and reduced fungal biomass in the HIGS wheat plants infected by CYR31 suggested that *PsCS1* is required for the growth and development of *Pst*, which could possibly be due to an insufficient supply of carbon sources and energy because the suppression of *PsCS1* resulted in the incomplete oxidation of nutrients absorbed from the host cells in *Pst*. However, there was no significant difference in the disease symptoms compared with the controls, indicating that the *Pst* pathogenicity was not fundamentally altered in *PsCS1*-knockdowned plants. This

could be because glycolysis and the acquisition of the necessary amino acids via haustoria (Voegele and Mendgen, 2011) ensure the basic metabolic requirements of *Pst*, although the development rate is impeded. Therefore, the silencing of *PsCS1* did not substantially affect the late-stage infection of *Pst*. These results indicate that PsCS1 is likely to contribute to fungal growth and development due to its energy and carbon source supply role but is not essential for *Pst* virulence.

In conclusion, this study revealed an important role of *PsCS1* during *Pst* infection of wheat. *PsCS1* encodes a novel mitochondria-localized CS that forms a homo-octamer and contributes to *Pst* infection by regulating ATP production and the supply of carbon sources.

Experimental Procedures

Plant materials, strains and culture conditions

The *Pst* pathotype CYR31 and the wheat cultivar Suwon 11 (Su11) were used in this study. Wheat cultivation and experimental inoculation of *Pst* were conducted as described by Kang *et al*. (2002). Fresh urediniospores were collected from the infected wheat leaves for extraction of total RNA and protein. To measure the *PsCS1* expression levels in the *Pst*-infected wheat leaves, the leaf tissues were sampled at indicated time points post inoculation.

Tobacco plants, which was used for transient overexpression mediated by *A. tumefaciens*, was grown in a growth chamber at 25°C under a light cycle of 16 h light/8 h darkness.

RNA extraction and qRT-PCR

Total RNA extraction and cDNA synthesis were performed as previously described (Liu *et al*., 2015). The expression levels of *PsCS1* were assayed at different *Pst* infection stages by qRT-PCR as previously described (Liu *et al*., 2016). The gene expression in *Pst* was normalized

using elongation factor-1 (EF-1) as an internal reference (Yin *et al*., 2009). The purity and specificity of the PCR products was confirmed by the SYBR green dissociation curve set up at the end of each PCR run. The significance of the differences between the time points was assessed using the following parameters, the relative quantity of RNA at least 2-fold higher or lower than the controls and $P \leq 0.005$.

The primers used for qRT-PCR are listed in Supporting Information Table S1.

Cloning of *PsCS1* and sequence analysis

To clone the *PsCS1* gene, the primers (Supporting Information Table S1) were designed on basis of the *PsCS1* coding sequence (CDS) from the complete genome sequence of *Pst* (Zheng *et al*., 2013). The *PsCS1* gene was amplified by PCR using a *Pst*-infected wheat cDNA sample as a template. The ProtParam tool at ExPASy (http://www.expasy.org/protparam/) was used to determine the physicochemical properties of PsCS1. The protein domain was analyzed based on the Pfam tool (http://pfam.sanger.ac.uk/). Target P (http://www.cbs.dtu.dk/services/TargetP/) was used for the prediction of the subcellular localization of PsCS1. The *PsCS1* gene copy number in the *Pst* genome was determined using BLASTN. Finally, the deduced amino acid sequence of PsCS1 was analyzed using BLASTP against non-redundant sequence databases (NCBI) to search homologous proteins. Some selected protein sequences were compared using ClustalW multialignment software. A neighbor-joining phylogenetic tree was constructed using software MEGA 7.0.

Plasmid construction

To biochemically characterize PsCS1, the CDS of *PsCS1* were amplified and cloned into the *Eco*RV/*Xho*I restriction sites of vector pET32a to obtain the recombinant plasmid pET32a-*PsCS1*.

To determine polymerization of PsCS1, the ORF of *PsCS1* was inserted into the *Eco*RI/*Bam*HI sites of pGADT7 and pGBKT7 to generate the recombinant constructs pGADT7-*PsCS1* and pGBKT7-*PsCS1*, respectively. In addition, *PsCS1* was also cloned into the *Bam*HI restriction site in the binary vectors pSPYCE(M) and pSPYNE(R)173 (Waadt *et al*., 2008) to obtain the recombinant plasmids pSPYCE(M)-*PsCS1* and pSPYNE(R)173-*PsCS1*, respectively.

To verify the subcellular localization of PsCS1, the ORF of *PsCS1* was amplified by PCR and cloned into pENTR/D-TOPO (Invitrogen). *PsCS1* was then recombined into the destination vector pK7FWG2 (Karimi *et al*., 2002) with a Gateway LR reaction following manufacturer's instructions (Invitrogen) so that the GFP was translationally fused with PsCS1 at its C termini.

Construction of the recombinant BSMV-HIGS vectors was performed as described by Holzberg *et al*. (2002). To specifically silence the *PsCS1* gene, the two γ RNA-based derivative plasmids *PsCS1*-as1 and *PsCS1*-as2 were constructed using a 245-bp fragment (nucleotides 161–405) and a 125-bp fragment (nucleotides 705–829) in an antisense orientation, which exhibited the highest polymorphism in the CS gene family of *Pst* and the lowest nucleotide sequence similarity with other genes from *Pst* and wheat.

The primers used for all constructs are listed in Supporting Information Table S1.

Preparation of crude extracts and citrate synthase enzyme assay

Germination of *Pst* urediniospores and total protein extraction were performed as previously described (Liu *et al*., 2014). The CS activity was measured according to the following reaction system: 520 μL buffer (50 mM Tris-HCl 1 mM EDTA and 100 mM KCl, pH 7.5), 20 μL acetyl coenzyme A (2.5 mM), 20 μL DTNB (5,5′-dithio-bis-2-nitrobenzoic acid, 5.025 mM) and 20 μL of the enzyme solution. The reaction was initiated by the addition of 20 μL oxaloacetate (5.0 mM)

after 5 min of preincubation at 25°C, and the absorbance at 412 nm was assayed using a spectrophotometer. The total protein levels were determined using a Coomassie Brilliant Blue G-250 protein assay reagent.

Expression of Trx-tagged fusion proteins and immunoblot analysis

The *E. coli* BL21(DE3) competent cells were transformed with the recombinant pET32a-*PsCS1* plasmid and the transformants were selected on LB plates supplemented with ampicillin (100 mg/L) at 37°C. The fusion protein was expressed by the induction of 1.0 mM IPTG for 10 h at 16°C. The harvested cells were lysed by sonication and the supernatant was analyzed by SDS-PAGE. The fusion protein was purified using a HisTrap HP affinity column and a Hitrap Q column (GE Healthcare, Uppsala, Sweden).

The Western blot analysis was performed as previously described (Liu *et al*., 2016). The purified fusion proteins were recognized by anti-His mouse monoclonal antibody and the nitrocellulose membrane was immunostained with diaminobenzidine (DAB) for 10 min in the dark.

Enzymatic characterization of PsCS1

The enzyme solutions were preincubated at 20–70°C and pH 3–11 for 30 min, respectively, to evaluate the thermal stabilities and pH optima of the purified enzyme. The residual enzyme activity of the abovementioned samples was measured at 30 min post treatment. The influences of five metal ions (0.5 mM Mn^{2+}, Cu^{2+}, Zn^{2+}, K^{+} or Fe^{3+}) on the CS activity of the purified PsCS1 were assayed. Enzyme solutions including each of the tested reagents were incubated for 30 min in 50 mM phosphate buffered saline (PBS, pH 7.8) at 25°C and the residual activity was detected as previously mentioned. Graphite furnace atomic absorption spectrometry was used to determine

the metal content in the purified PsCS1 after the enzyme solution was dialyzed adequately against 50 mM Tris-HCl (pH 7.5) containing 1 mM EDTA and then in EDTA-free buffer. Biological replicates were performed in triplicate.

Size-exclusion chromatography analysis of PsCS1

The N-terminal Trx tags of the purified fusion proteins were removed by thrombin digestion. The native molecular mass of PsCS1 was then determined using size exclusion chromatography. The samples were loaded into a Superdex^{TM}200 column (GE Healthcare) equilibrated in 20 mM Tris-HCl buffer, pH 8.0, containing 200 mM NaCl at a flow rate of 0.3 mL/min for preparative-scale fractionation. Protein fractions were collected based on UV absorbance at 280 nm and the elution times. The column was calibrated by chromatographic protein standards (thyroglobulin, 670 kDa; globulin, 158 kDa; ovalbumin, 44 kDa; myoglobin, 17 kDa, and vitamin B12, 1.35 kDa).

Yeast two-hybrid assays

PsCS1 interactions with itself were investigated by co-transformation of the plasmids pGBKT7-*PsCS1* and pGADT7-*PsCS1* into the yeast cell "Y2H Gold" (Clontech) using the lithium acetate method (Gietz and Woods, 2002). Transformed cells were cultured on synthetic complete (SC) media lacking Trp and Leu for 3 days at 30°C. Single colonies were suspended in the SD-Leu-Trp medium, and serial 1:10 dilutions were plated in either SD (synthetic dropout)-Leu-Trp (SD-LT), SD-Leu-Trp-His (SD-LTH), SD-Leu-Trp-His-Ade (SD-LTAH) or SD-LTAH+X-α-Gal media. Cell growth was observed 3 days after plating. The yeast cell line expressing the empty vector pGADT7 with pGBKT7-*PsCS1* was used as a negative control.

Split GFP assay

Bimolecular fluorescence complementation experiments were performed as previously described (Xuan *et al*., 2013). Agrobacteria carrying the recombinant plasmid pSPYNE(R)173-*PsCS1* or pSPYCE(M)-*PsCS1* were co-infiltrated into tobacco leaves. After 48 h, self-interaction of PsCS1 was determined by monitoring yellow fluorescent protein (YFP) signals by confocal microscope. At least three biological repeats were performed with comparable results.

Subcellular localization of PsCS1 in *N. benthamiana*

To determine the subcellular localization of PsCS1, tobacco leaves were infiltrated with the culture of an *A. tumefaciens* strain GV3101 harboring pK7FWG2-*PsCS1* and analyzed after 2 d. cd3-991 and cd3-983 were used to label the mitochondria and peroxisome (Nelson *et al*., 2007). A Zeiss LSM510 META confocal microscope was used to monitor GFP and mCherry fluorescence signals.

Study of *E. coli* cells with PsCS1 during different types of abiotic stress

A spot assay was conducted to determine the response of *E. coli* BL21(DE3) cells carrying the recombinant plasmid pET32a-*PsCS1* or the empty vector pET32a to NaCl and H_2O_2 stress. When the cells grew to 0.6 (OD_{600}) in LB medium, IPTG induction was performed as described above. Serial 10-fold dilutions of the cultures (OD_{600}=0.6) were prepared, and 10 μL of each dilution was spotted onto LB plates containing 50, 150 and 250 mM NaCl, or 0, 0.2, 0.5, 1.0 and 2.0 mM H_2O_2. The growth of *E. coli* cells with PsCS1 was also measured at different temperature. All the LB basal plates contained 50 mg/L ampicillin.

In addition, the growth of *E. coli* carrying the recombinant pET32a-*PsCS1* plasmid or pET32a was studied in liquid media supplemented with NaCl or PEG6000. *E. coli* cells were cultured as described earlier and diluted to 0.6 (OD_{600}). Approximately 400 μL of the cells were

inoculated into 25 mL of LB medium containing 250 mM NaCl or 20% PEG6000 and shaken at 200 rpm at 37°C with growth measurement harvests every 2 h.

BSMV-mediated *PsCS1* silencing during the wheat-*Pst* interaction

To silence the *PsCS1*, two recombinant viruses (BSMV:*PsCS1*-as1 and BSMV:*PsCS1*-as2) were employed to inoculate wheat seedlings as previously described (Liu *et al*., 2016). 1 × FES - buffer-inoculated wheat seedlings acted as the mock control. BSMV:γ and BSMV:*TaPDS* were used as the controls for the virus infection. In general, 18 wheat plants were required for each assay. BSMV-inoculated wheat seedlings were incubated at 23±2°C in a plant growth chamber. At 9 d after virus inoculation, the fourth leaves were further infected with the *Pst* pathotype CYR31, and sampled at 0, 24, 48, and 120 hpi for RNA extraction and histological observation (Wang *et al*., 2007). The disease phenotypes were recorded and photographed at 15 dpi. The silencing efficiency of *PsCS1* was quantified by qRT-PCR. In addition, the transcript levels of two wheat CS genes *TaCS1* (GenBank accession number KU821107) and *TaCS2* (GenBank accession number AK455004) were also detected using qRT-PCR in the HIGS plants. Biological replicates were performed in triplicate.

The changes in fungal biomass were measured as previously described (Liu *et al.*, 2016). The quantification of the *Pst* and wheat genomic DNA in *Pst*-infected wheat samples, and the calculation of the relative quantities were performed based on the standard curves constructed (Liu *et al.*, 2016).

The primers used are listed in Supporting Information Table S1.

Histological observation of fungal growth

To identify the function of *PsCS1* during the *Pst* infection of wheat, the fungal development

was observed microscopically in the *PsCS1*-silenced wheat plants. The leaf segments sampled for histological observation were fixed and stained with wheat germ agglutinin conjugated to Alexa Fluor-488 (Invitrogen) as described previously (Wang *et al*., 2007). Haustorial mother cells, haustoria, hyphal length and branches as well as colony size were analyzed statistically as previously described (Liu *et al*., 2016). Five leaf segments were randomly selected and no less than 50 infection sites were examined for each treatment.

Acknowledgements

This study was supported by the National Key Research and Development Program of China (2016YFD0100602), the 111 Project of the Ministry of Education of China (B07049) and the Chinese Universities Scientific Fund (2452018151).

References

Aftab Hussain, A., Pavithra, I.S., Sreevathsa, R., Nataraja, K.N., and Babu, N. (2016) Development of transgenic pigeonpea [*Cajanus cajan* (L.) Millsp.] overexpressing citrate synthase gene for high phosphorus uptake. *Indian J Exp Biol* **54**: 493–501.

Alekseev, K.V., Dubina, M.V., and Komov, V.P. (2016) Molecular-genetic and biochemical characteristics of citrate synthase from the citric-acid producing fungus *Aspergillus niger*. *Appl Biochem Microbiol* **52**: 810–817.

Ayliffe, M., Devilla, R., Mago, R., White, R., Talbot, M., Pryor, A., *et al.* (2010) Nonhost resistance of rice to rust pathogens. *Mol Plant Microbe Interact* **24**: 1143–1155.

Barone, P., Rosellini, D., Lafayette, P., Bouton, J., Veronesi, F., and Parrott, W. (2008) Bacterial citrate synthase expression and soil aluminum tolerance in transgenic

alfalfa. *Plant Cell Rep* **27**: 893–901.

Bastos, K.P., Bailão, A.M., Borges, C.L., Faria, F.P., Felipe, M.S., Silva, M.G., *et al.* (2007) The transcriptome analysis of early morphogenesis in *Paracoccidioides brasiliensis*, mycelium reveals novel and induced genes potentially associated to the dimorphic process. *BMC Microbiol* **7**: 1–14.

Chen, V.C., Sadler, G., Mccomb, M.E., Perreault, H., and Duckworth, H.W. (2011) Characterization of specific binding by mass spectrometry: Associations of *E. coli* citrate synthase with NADH and 2-azidoATP. *Int J Mass Spectrom* **305**: 238–246.

de la Fuente, J.M., Ramírez-Rodríguez, V., Cabrera-Ponce, J.L., and Herrera-Estrella, L. (1997) Aluminum tolerance in transgenic plants by alteration of citrate synthesis. *Science* **276**: 1566–1568.

Ferea, T., Contreras, E.T., Oung, T., Bowman, E.J., and Bowman, B.J. (1994) Characterization of the cit-1 gene from *Neurospora crassa* encoding the mitochondrial form of citrate synthase. *Mol Gen Genet* **242**: 105–110.

Gietz, R.D., and Woods, R.A. (2002) Transformation of yeast by lithium acetate/single-stranded carrier DNA/polyethylene glycol method. *Method Enzymol* **350**: 87–96.

Goldenthal, M.J., Marin-Garcia, J., and Ananthakrishnan, R. (1998) Cloning and molecular analysis of the human citrate synthase gene. *Genome* **41**: 733–738.

Guest, J. R. (1981) Hybrid plasmids containing the citrate synthase gene (glt4) of *Escherichia coli* K12. *J Gen Microbiol* **124**: 17–23.

Hao, Y.B., Wang, T., Wang, K., Wang, X.J., Fu, Y.P., Huang, L.L., *et al.* (2016)

Transcriptome analysis provides insights into the mechanisms underlying wheat plant resistance to stripe rust at the adult plant stage. *PLoS One* **11**: e0150717.

Holzberg, S., Brosio, P., Gross, C., and Pogue, G.P. (2002) Barley stripe mosaic virus-induced gene silencing in a monocot plant. *Plant J* **30**: 315–327.

Jia, Y.K., Becam, A.M., and Herbert, C.J. (1997) The CIT3 gene of *Saccharomyces cerevisiae* encodes a second mitochondrial isoform of citrate synthase. *Mol Microbiol* **24**: 53–59.

Kang, J.M., Xie, W.W., Sun, Y., Yang, Q.C., and Wu, M.S. (2010) Identification of genes induced by salt stress from *Medicago truncatula* L. seedlings. *Afr J Biotechnol* **9**: 7589–7594.

Kang, Z.S., Huang, L.L., and Buchenauer, H. (2002) Ultrastructural changes and localization of lignin and callose in compatible and incompatible interactions between wheat and *Puccinia striiformis*. *Zeitschrift Für Pflanzenkrankheiten Und Pflanzenschutz*. **109**: 25–37.

Karimi, M., Inze, D., and Depicker, A. (2002) GATEWAY vectors for *Agrobacterium*-mediated plant transformation. *Trends Plant Sci* **7**: 193–195.

Kim, K.S., Rosenkrantz, M.S., and Guarente, L. (1986) *Saccharomyces cerevisiae* contains two functional citrate synthase genes. *Mol Cell Biol* **6**: 1936–1942.

Kosicki, G.W., and Lee, L.P. (1966) Effect of divalent metal ions on nucleotide inhibition of pig heart citrate synthase. *J Biol Chem* **241**: 3571.

Koyama, H., Kawamura, A., Kihara, T., Hara, T., Takita, E., and Shibata, D. (2000) Overexpression of mitochondrial citrate synthase in *Arabidopsis thaliana* improved

growth on a phosphorus-limited soil. *Plant Cell Physiol* **41**: 1030–1037.

Koyama, H., Takita, E., Kawamura, A., Hara, T., and Shibata, D. (1999) Over expression of mitochondrial citrate synthase gene improves the growth of carrot cells in Al-phosphate medium. *Plant Cell Physiol* **40**: 482–488.

Lewin, A.S., Hines, V., and Small, G.M. (1990) Citrate synthase encoded by the CIT2 gene of *Saccharomyces cerevisiae* is peroxisomal. *Mol Cell Biol* **10**: 1399–1405.

Liu, J., Guan, T., Zheng, P.J., Chen, L. Y., Yang, Y., Huai, B.Y., *et al*. (2016) An extracellular Zn-only superoxide dismutase from *Puccinia striiformis* confers enhanced resistance to host-derived oxidative stress. *Environ Microbiol* **18**: 4118–4135.

Liu, J., Wang, Q.L., Chang, Q., Han, L.N., Pei, G.L., Xue, Y.Q., *et al*. (2014) Isocitrate lyase is required for urediniospore germination of *Puccinia striiformis* f. sp. *tritici*. *Mol Biol Rep* **41**: 7797–7806.

Liu, J.H., Chi, G.H., Jia, C.H., Zhang, J.B., Xu, B.Y., and Jin, Z.Q. (2013) Function of a citrate synthase gene (MaGCS) during postharvest banana fruit ripening. *Postharvest Biol Technol* **84**: 43–50.

Maeda, H., Sano, M., Maruyama, Y., Tanno, T., Akao, T., Totsuka, Y., *et al.* (2004) Transcriptional analysis of genes for energy catabolism and hydrolytic enzymes in the filamentous fungus *Aspergillus oryzae*, using cDNA microarrays and expressed sequence tags. *Appl Microbiol Biotechnol* **65**: 74–83.

Mcevily, A.J., and Harrison, J.H. (1986) Subunit equilibria of porcine heart citrate synthase. Effects of enzyme concentration, pH, and substrates. *J Biol Chem* **261**:

2593–2598.

Min, I.S., Bang, J.Y., Seo, S.W., Lee, C.H., and Maeng, P.J. (2010) Differential expression of citA gene encoding the mitochondrial citrate synthase of *Aspergillus nidulans* in response to developmental status and carbon sources. *J Microbiol* **48**: 188–198.

Nelson, B.K., Cai, X., and Nebenführ, A. (2007) A multicolored set of in vivo organelle markers for co-localization studies in *Arabidopsis* and other plants. *Plant J* **51**: 1126–1136.

Park, B.W., Han, K.H., Lee, C.Y., Lee, C.H., and Maeng, P.J. (1997) Cloning and characterization of the citA gene encoding the mitochondrial citrate synthase of *Aspergillus nidulans*. *Mol Cells* **7**: 290–295.

Pracharoenwattana, I., Cornah, J.E., and Smith, S.M. (2005) *Arabidopsis* peroxisomal citrate synthase is required for fatty acid respiration and seed germination. *Plant Cell* **17**: 2037–2048.

Rosenkrantz, M., Alam, T., Kim, K.S., Clark, B.J., Srere, P.A., and Guarente, L.P. (1986) Mitochondrial and nonmitochondrial citrate synthases in *Saccharomyces cerevisiae* are encoded by distinct homologous genes. *Mol Cell Biol* **6**: 4509–4515.

Schmidtmann, E., König, A.C., Orwat, A., Leister, D., Hart, M., and Finkemeier, I. (2014) Redox regulation of *Arabidopsis* mitochondrial citrate synthase. *Mol Plant* **7**: 156–169.

Schnarrenberger, C., and Martin, W. (2002) Evolution of the enzymes of the citric acid cycle and the glyoxylate cycle of higher plants. *Eur J Biochem* **269**: 868–883.

Sheldon, J.R., Marolda, C.L., and Heinrichs, D.E. (2014) TCA cycle activity in *Staphylococcus aureus* is essential for iron-regulated synthesis of staphyloferrin A, but not staphyloferrin B: the benefit of a second citrate synthase. *Mol Microbiol* **92**: 824–839.

Suissa, M., Suda, K., and Schatz, G. (1984) Isolation of the nuclear yeast genes for citrate synthase and fifteen other mitochondrial proteins by a new screening method. *EMBO J* **3**: 1773–1781.

Tong, J., Zhan, G.M., Wang, X.F., Liu, G.H., Hua, W., and Wang, H.Z. (2009) Cloning of citrate synthase gene in Rapeseed (*Brassica napus* L.) and its expression under stresses. *Acta Agronomica Sinica* **35**: 33–40.

Unger, E.A., Hand, J.M., Cashmore, A.R., and Vasconcelos, A.C. (1989) Isolation of a cDNA encoding mitochondrial citrate synthase from *Arabidopsis thaliana*. *Plant Mol Biol* **13**: 411–418.

Vargas, W.A., Pontis, H.G., and Salerno, G.L. (2007) Differential expression of alkaline and neutral invertases in response to environmental stresses: characterization of an alkaline isoform as a stress-response enzyme in wheat leaves. *Planta* **226**: 1535–1545.

Voegele, R.T., and Mendgen, K. (2003) Rust haustoria: nutrient uptake and beyond. *New Phytol* **159**: 93–100.

Voegele, R.T., and Mendgen, K.W. (2011) Nutrient uptake in rust fungi: how sweet is parasitic life? *Euphytica* **179**: 41–55.

Waadt, R., Schmidt, L.K., Lohse, M., Hashimoto, K., Bock, R., and Kudla, J. (2008)

Multicolor bimolecular fluorescence complementation reveals simultaneous formation of alternative CBL/CIPK complexes in planta. *Plant J* **56**: 505–516.

Wang, C.F., Huang, L.L., Buchenauer, H., Han, Q.M., Zhang, H.C., and Kang, Z.S. (2007) Histochemical studies on the accumulation of reactive oxygen species ($O^{2\bullet}$ and H_2O_2) in the incompatible and compatible interaction of wheat–*Puccinia striiformis* f. sp. *tritici*. *Physiol Mol Plant P* **71**: 230–239.

Weitzman, P.D., and Dunmore, P. (1969) Citrate synthases: allosteric regulation and molecular size. *Biochim Biophys Acta* **171**: 198–200.

Weitzman, P.D., and Jones, D. (1968) Regulation of citrate synthase and microbial taxonomy. *Nature* **219**: 270–272.

Xuan, Y.H., Hua, Y.B., Chen, L.Q., Sosso, D., Ducat, D.C., Hou, B.H., *et al.* (2013) Functional role of oligomerization for bacterial and plant SWEET sugar transporter family. *Proc Natl Acad Sci USA* **110**: E3685–E3694.

Yin, C.T., Chen, X.M., Wang, X.J., Han, Q.M., Kang, Z.S., and Hulbert, S.H. (2009) Generation and analysis of expression sequence tags from haustoria of the wheat stripe rust fungus *Puccinia striiformis* f. sp. *tritici*. *BMC Genomics* **10**: 626.

Yue, C.P., Zhang, N.N., An, L.P., Wang, Q.D., and Huang, J.Y. (2014) Cloning and expression of citrate synthase gene of *Sinapis alba* under drought stress. *Life Sci J* **11**: 163–167.

Zhao, H., Jia, F.Q., Zhang, F.C., and Wang, Y. (2014) The transcriptome information analysis of differentially expressed genes of *Halostachys caspica* under salt stress. *Chinese Journal of Bioinformatic*s **24**: 443–460.

Zhao, J., Wang, M., Chen, X.M., and Kang, Z.S. (2016) Role of alternate hosts in epidemiology and pathogen variation of cereal rusts. *Annu Rev Phytopathol* **54**: 207–228.

Zheng, W.M., Huang, L.L., Huang, J.Q., Wang, X.J., Chen, X.M., Zhao, J., *et al.* (2013) High genome heterozygosity and endemic genetic recombination in the wheat stripe rust fungus. *Nat Commun* **4**: 2673.

Figure legends

Fig. 1. A. The expression level of *PsCS1* at different *Pst* infection stages. The transcript levels of *PsCS1* were calculated by the comparative Ct method using *PsEF-1* as the internal reference. The relative quantifications were compared with the transcript abundance in nongerminated urediniospores. The means and standard deviations were calculated from three bilogical replicates. B. Analysis of citrate synthase enzyme activity in nongerminated and germinated urediniospores. US, urediniospores; GT, germ tubes.

Fig. 2. Purification and biochemical characteristics of PsCS1 expressed in *E. coli*

A. The SDS-PAGE profiles of PsCS1 expressed in *E. coli* cells. Lane 1, cell lysates of uninduced *E. coli* carrying pET32a; lane 2, cell lysates of *E. coli* carrying pET32a induced by IPTG; lane 3, cell lysates of uninduced *E. coli* carrying pET32a-*PsCS1*; lanes 4–6, cell lysates of *E. coli* carrying pET32a-*PsCS1* induced by IPTG. Lanes 4, 5, and 6 indicate whole-cell lysates, soluble fractions, and insoluble fractions, respectively; lane 7, purified Trx-PsCS1 proteins; M, marker. Thermal (B) and pH (C) stability of the purified PsCS1. D. Influences of different metal ions on the enzyme activity of the purified PsCS1. Asterisks represent a statistically significant difference from corresponding control samples (P<0.05) .

Fig. 3. A. Determination of the molecular weight of PsCS1. Gel filtration was performed on a HiPrep Sephacryl S-200 HR column. Standard proteins: a Thyroglobulin (670 kDa), b globulin (158 kDa), c Ovalbumin (44 kDa), d Myoglobin (17 kDa), and e vitamin B12 (1.35 kDa). The arrow indicates the elution volume of PsCS1. B. Yeast two-hybrid analyses show that PsCS1 interacts with itself in yeast. Growth on SD–LW confirms the presence of both bait and prey vectors. Growth on SD–LWHA and coloration on SD–LWHA supplemented with X-α-gal

confirms the bait and prey interaction. C. Self-interaction of PsCS1 in *Nicotiana benthamiana*. BiFC complexes formed by Agrobacterium infiltration in *N. benthamiana* leaves were observed using confocal microscope after 3 days.

Fig. 4. Subcellular localization of PsCS1 in *Nicotiana benthamiana*.

Co-expression of the PsCS1:GFP fusion protein with mCherry markers for mitochondria (A) and peroxisome (B) in epidermal leaf cells of *N. benthamiana*. The GFP and mCherry fluorescence signals were monitored using confocal microscopy. Bars=10 μm.

Fig. 5. A. A spot assay of *E. coli* harboring pET32a or pET32a-*PsCS1* on LB plates with NaCl. B. Liquid culture assay of *E. coli*/pET32a-*PsCS1* in LB media with 250 mM NaCl. The *E. coli* harboring pET32a empty vector was used as the control. The overexpression of *PsCS1* significantly enhanced *E. coli* resistance to salt stress compared with the control. Biological replicates were conducted in triplicate.

Fig. 6. Silencing of *PsCS1* in the wheat-*Pst* interaction using BSMV-HIGS results in restricted *Pst* growth. The results shown are mean ± SD from three independent experiments. Asterisks represent a statistically significant difference from corresponding control samples ($P<0.05$). (A) Chlorotic and mosaic phenotypes were visualized on the fourth wheat leaves inoculated with BSMV at 9 dpi, and photo-bleaching was significantly observed on the fourth wheat leaves inoculated with BSMV:*TaPDS*. CK, the FES buffer-inoculated wheat leaves. (B) Disease symptoms of the fourth leaves preinoculated with BSMV and then infecteded with CYR31. (C) Fungal biomass was measured using real-time quantitative PCR analysis of the total DNA isolated from the *Pst*-infected wheat leaves at 7 dpi. *TaEF-1a* and *PsEF1* were used to assess the ratio of the total *Pst* DNA to the total wheat DNA. (D). The silencing efficiency of *PsCS1* was evaluated

using qRT-PCR. The BSMV:γ-inoculated wheat leaves infected with *Pst* served as the controls. *PsEF1* was used to normalize the expression of *PsCS1*.

Fig. 7. Fungal growth was histologically observed in *Pst*-infected wheat leaves after inoculation with BSMV:γ and recombinant BSMV. (A–F) Fungal development at 24 (A) or 48 hpi (B), colony size at 120 hpi per infection site (C) in BSMV:γ-infected plants. (D–F) Fungal growth at 24 hpi (D) or 48 hpi (E), infection unit area at 120 hpi (F) in BSMV:*PsCS1*-infected plants. (G) The average number of hyphal branches (HB), haustorial mother cells (HMC) and haustoria (H) at 24 hpi showed little change in the HIGS plants infected by CYR31. (H) Colony size per infection site was significantly decreased in HIGS wheat plants infected by CYR31 at 120 hpi. Values are representative of the mean ± standard error of three independent experiments. Differences of means were evaluated using Student's *t*-tests and asterisks indicate significant difference ($P<0.05$) compared with the control. SV, substomatal vesicle; IH, infection hypha.

Fig. 1

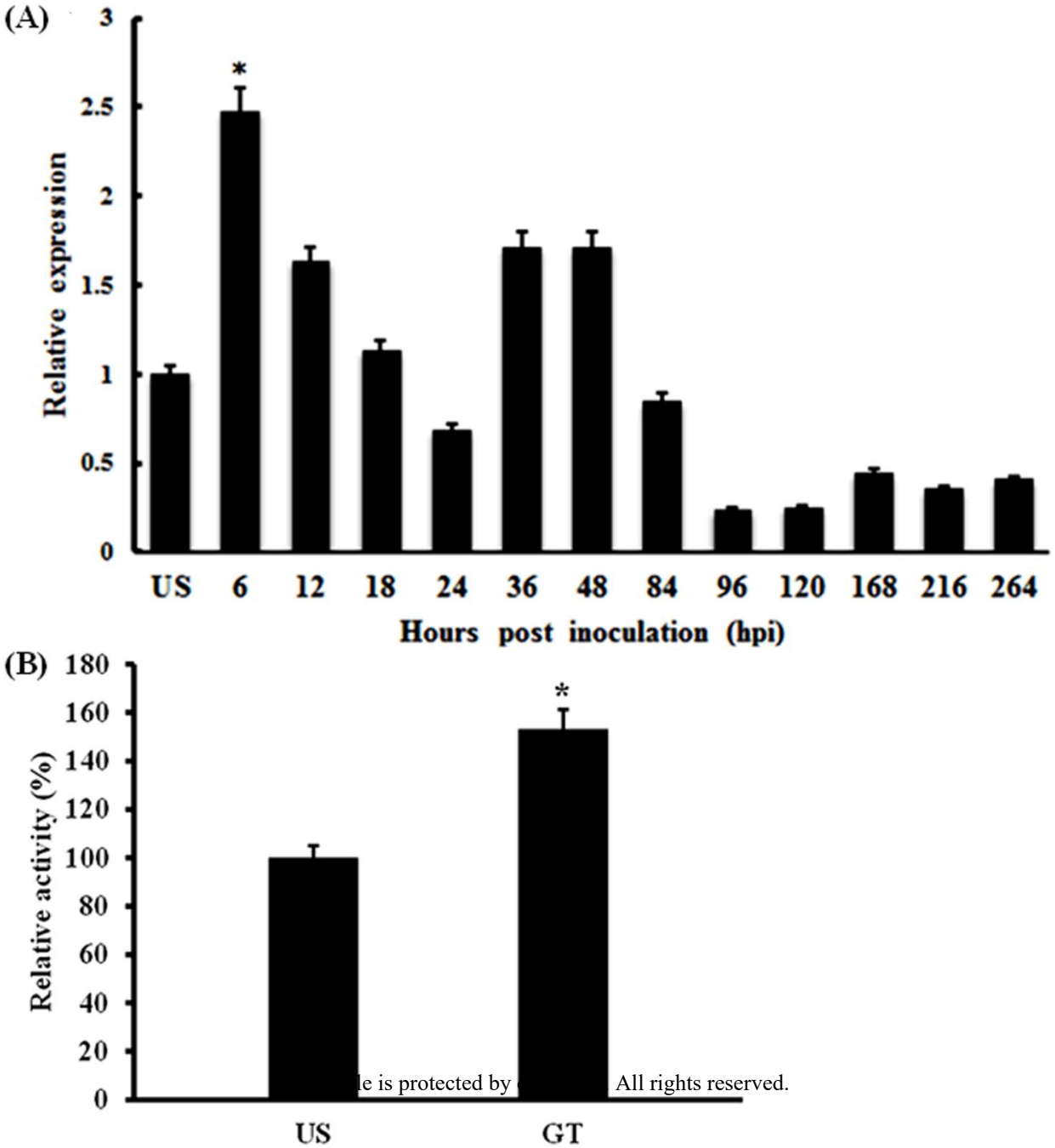

Fig. 2

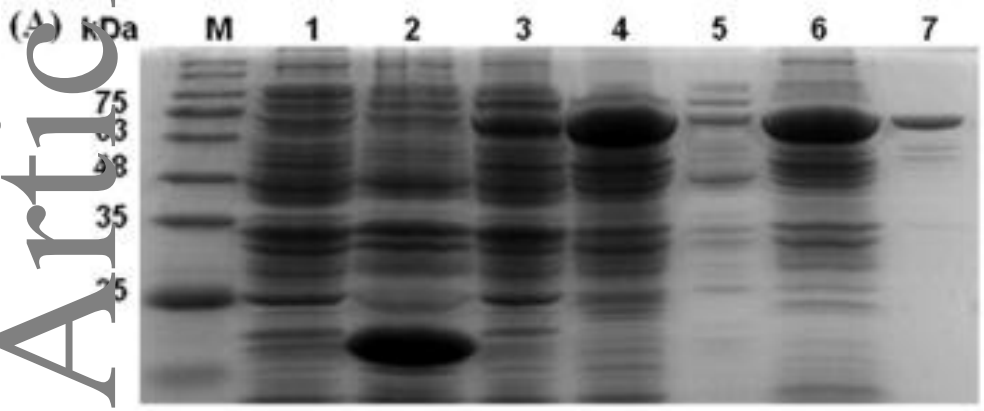

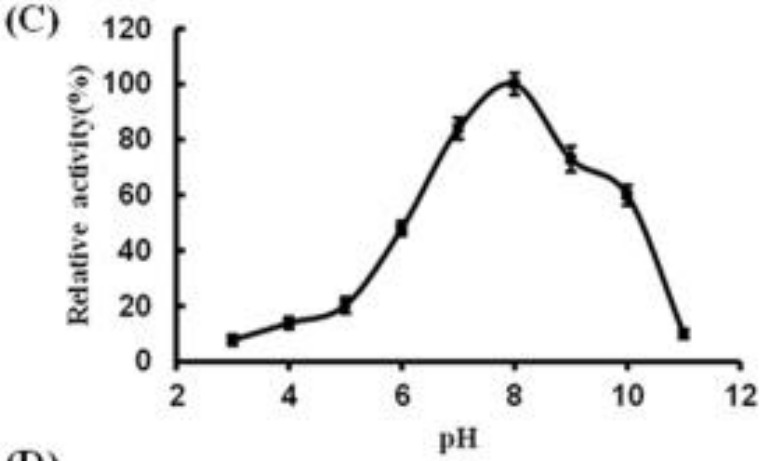

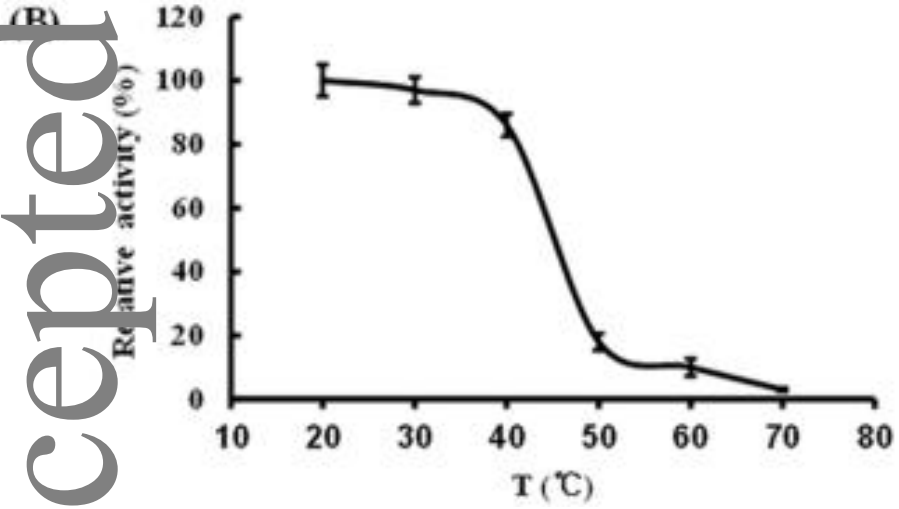

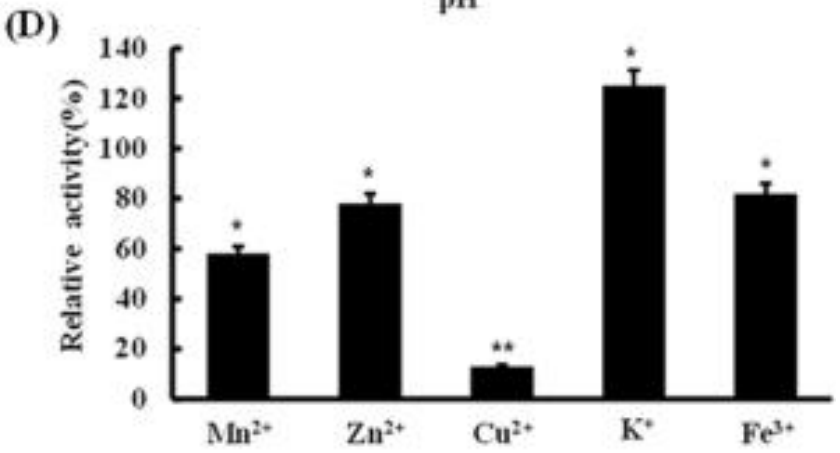

Fig. 3

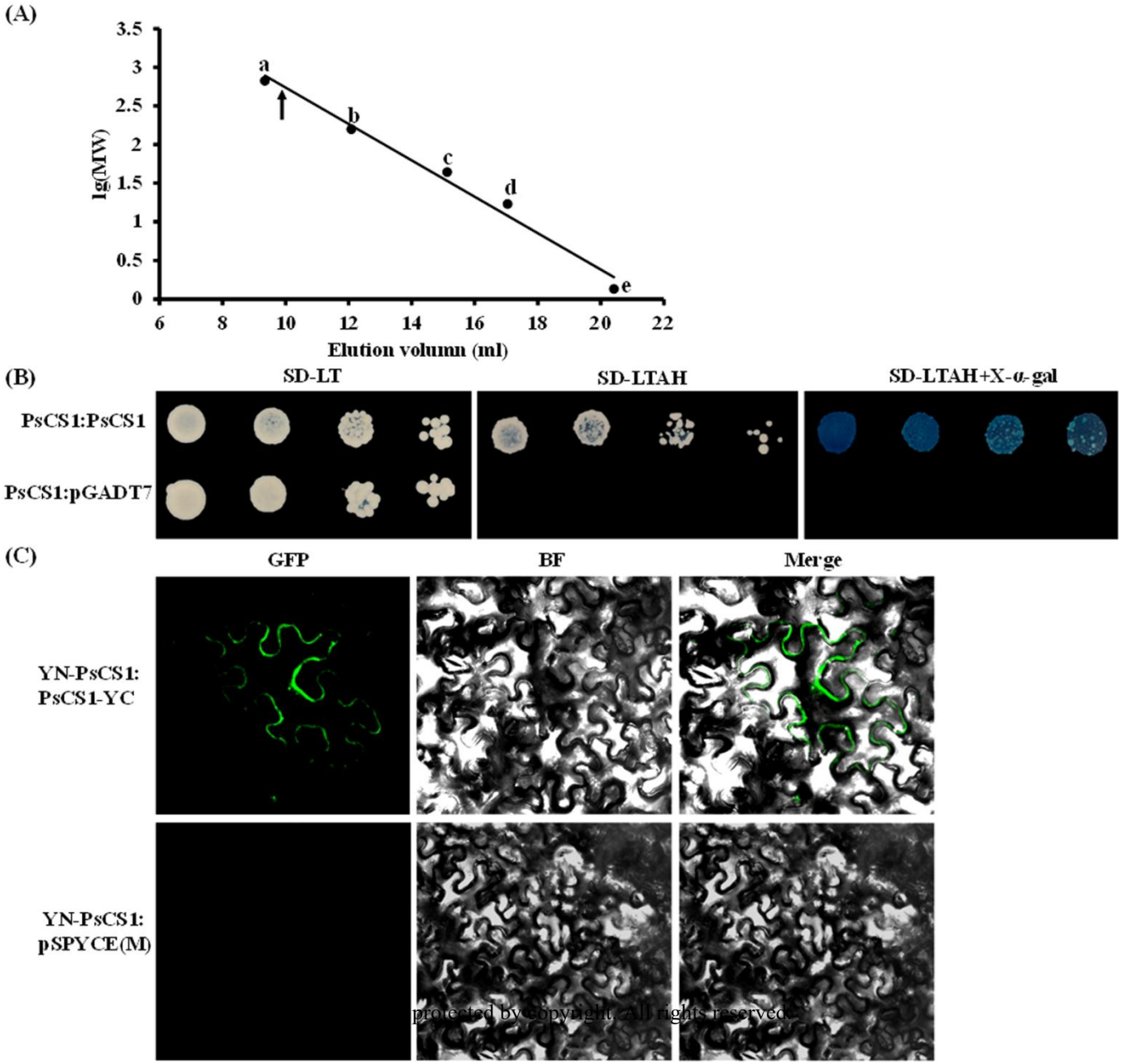

Fig. 4

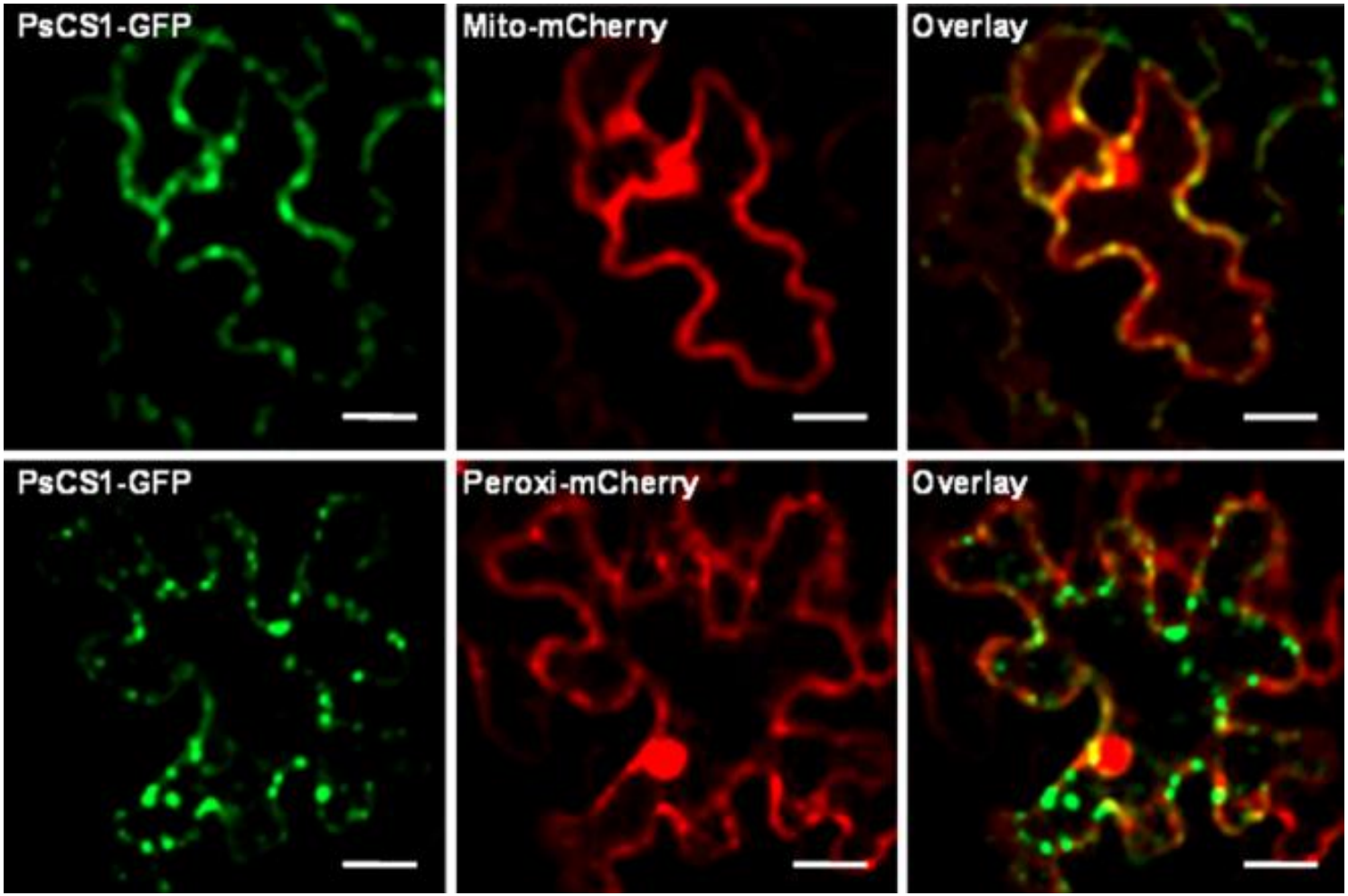

Fig. 5

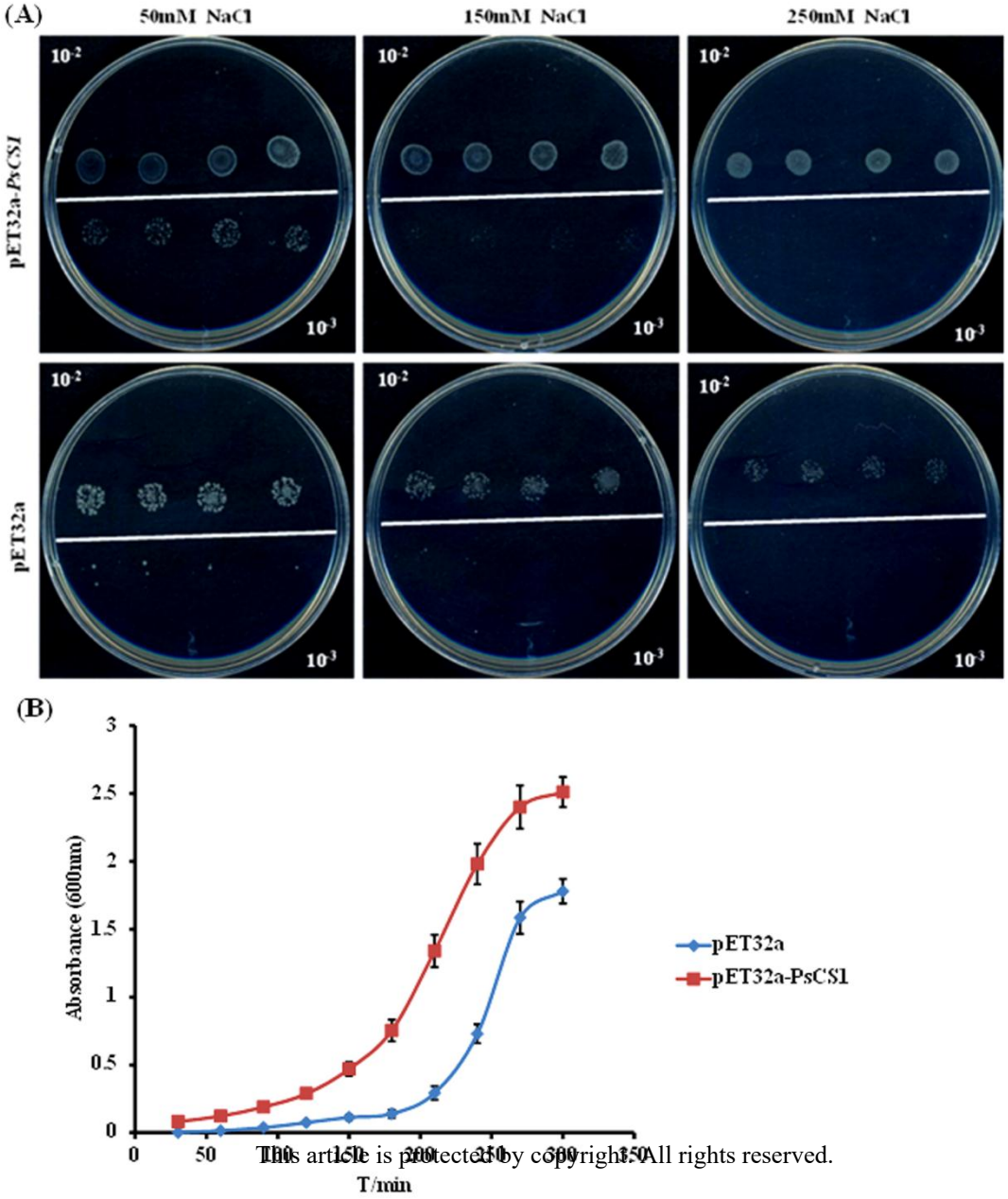

Fig. 6

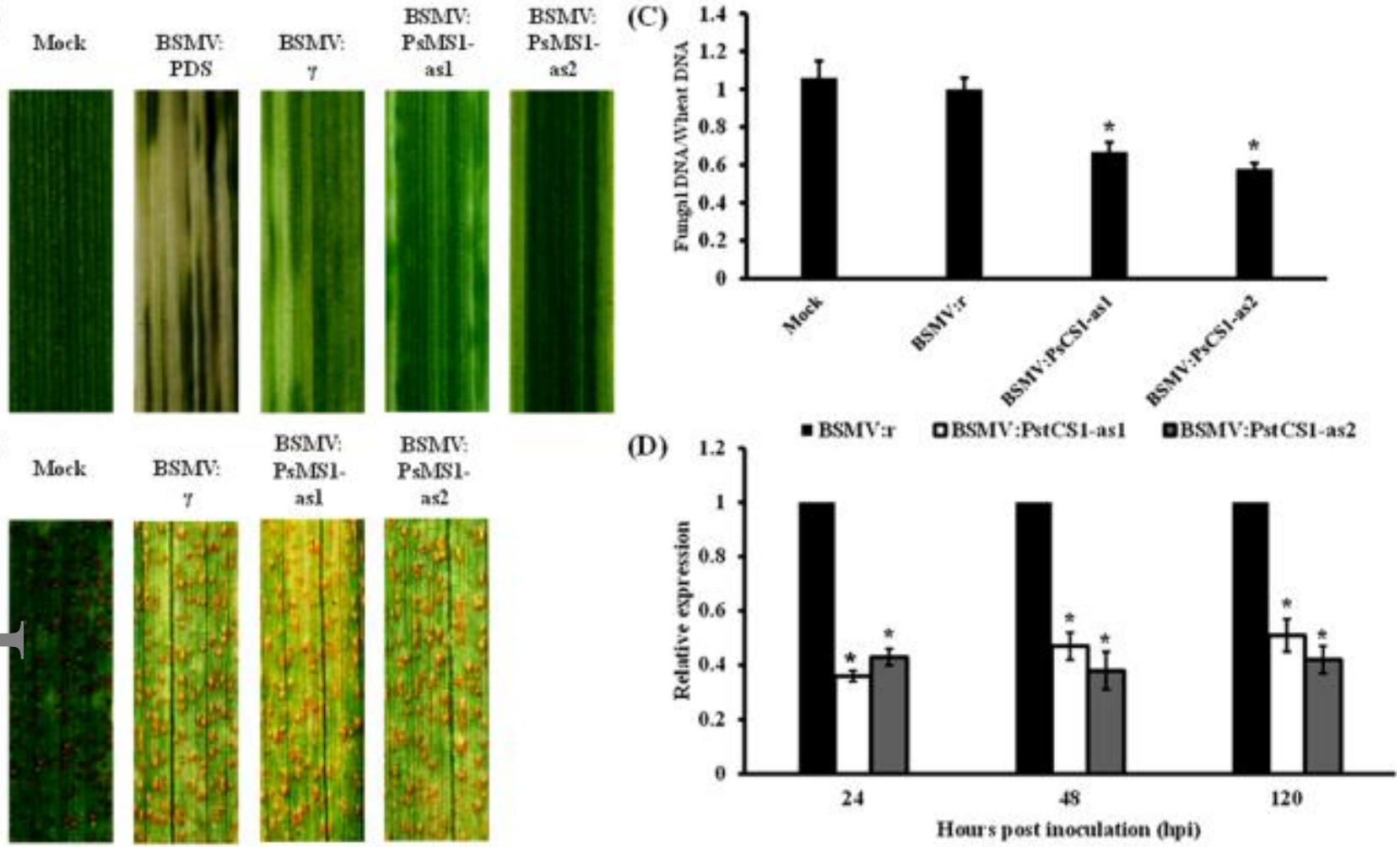

Fig. 7